Electrochimica Acta 147 (2014) 47–53

Contents lists available at ScienceDirect

Electrochimica Acta

journal homepage: www.elsevier.com/locate/electacta

The electrodeposition of Ga-doped $CuInSe_2$ thin film in the presence of Triton 100-X

F. Willian de S. Lucas, Alan R.F. Lima, Lucia H. Mascaro *

Department of Chemistry, Federal University of São Carlos, São Carlos, São Paulo 13565-905, Brazil

ARTICLE INFO

Article history:
Received 28 July 2014
Received in revised form 17 September 2014
Accepted 20 September 2014
Available online 29 September 2014

Keywords:
Solar cell
chalcopyrite
CIGSe
semiconductor electrodeposition

ABSTRACT

The codeposition of Cu, In, Ga and Se from pH 1.5 at Na_2SO_4/H_2SO_4 solution onto fluorine doped tin oxide (FTO) was studied. The effects of Triton 100-X as a noncomplexing and nonionic additive in the electrodeposition process was evaluated. At optimised experimental conditions was possible to obtain of Ga-doped $CuInSe_2$ films (CIGSe). The films presented two different morphologies, one layer formed by globular structures and another layer constituted of lamellar clusters. The major phase in the films was CIGSe, but binary phases as InSe and CuSe were also identified. The value of the band gap was at about 1.35 eV for all the films. It was observed that the additive presence in electrolytic bath reduces the number of surface defects and increases the crystallinity and purity of the electrodeposited CIGSe.

1. Introduction

Many researchers have shown that solar photovoltaic energy conversion is one of the main energy sources of the future. Solar energy is inexhaustible, has renewable characteristics, and is considered to be a clean energy source. To obtain maximum efficiency and low cost, several technological variations have been adopted that highlight the use of photovoltaic modules made of thin films of semiconductors. Among these semiconductors, the chalcopyrites family specifically, the Ga-doped $CuInSe_2$ (CIGSe) have shown the highest efficiency for solar cells in both laboratory and on an industrial scale. The maximum efficiency of these devices registered on a laboratory scale was 20.1% [1]. Thin film of CIGSe is a promising semiconductor material as an absorbent layer in a solar cell [2] and photoelectrochemical hydrogen production application [3]. The band gap of this quaternary semiconductor varies between 1.04 eV and 1.68 eV (1.04 eV to $CuInSe_2$ and 1.68 eV to $CuGaSe_2$). This material also exhibits a high absorption coefficient of $>10^5\,cm^{-1}$ at photon energies above the band gap, which makes it ideal for the fabrication of high efficiency thin film photovoltaic devices [2]. The most widely employed and successful technique for the deposition of the chalcopyrite layer is 'coevaporation', the vacuum-based approach, in which the film is formed in a single step [2,4]. A vast number of possible low-cost strategies for CIGSe thin film solar cells have been described to replace the direct deposition of photovoltaic quality films with a two-step process. Firstly, a precursor layer is prepared using a low-cost method which does not exhibit suitable electronic properties. Then, these properties are improved in a second functionalization step, which is generally based on a specific thermal treatment. Thus, the optimisation of the precursor film properties (composition, structure) and the functionalization step (temperature, pressure, atmosphere, duration of the annealing) should lead to the final electronic quality of the material comparable to that achieved in a one-step process [4]. Among the different low-cost methods, the most intensely investigated and striking strategy may be electrodeposition. It is simple, economical, viable and capable of producing good quality films with a large area in various geometries and with a low deposition temperature. It is possible to control the thickness and composition by adjusting the conditions of electrolysis and the components of the deposition bath [2,5].

Using the strategy mentioned above, in 1997, Bhattacharya et al. of the National Renewable Energy Laboratory (NREL) obtained a new efficiency record of 12.3% using a hybrid 'electrodeposition/evaporation' approach to obtain the CIGSe film absorber [6]. Bhattacharya et al. improved the process, and in 1998, Cu-rich CIGSe film obtained by electrodeposition as first step achieved an efficiency of 14.1% [7]. In 1999, efficiency improved to 15.4% [8].

It is important to understand and control the processes of semiconductor electrodeposition (the first step is obtaining good-quality film using a low-cost method) to obtain nanostructures that improve or add new optoelectronic properties to the films. The use of additives in electrodeposition can have interesting effects on the growth and structure of the films. No study has focused on the effect of nonionic and noncomplexing additives in the electrodeposition of CIGSe thin film. As a nonionic and noncomplexing

* Corresponding author. Tel.: +55 16 3361 8082.
E-mail address: lmascaro@ufscar.br (L.H. Mascaro).

http://dx.doi.org/10.1016/j.electacta.2014.09.097
0013-4686/

additive, Triton 100-X (TRT) has been used in alloy plating, resulting in higher deposition efficiency and improvement in the microstructure of deposits [9]. In this work, analysis by cyclic voltammetry, Raman spectroscopy, energy dispersive X-ray, NIR-UV-vis spectroscopy, scanning electron microscopy, Mott-Schottky and Rietveld refinement of the X-ray diffraction patterns provide insight into the effects of the TRT on electrodeposition of CIGSe thin films.

2. Experimental

2.1. Chemicals and apparatus

All chemicals used were of analytical grade and underwent no further purification: isopropanol (Alfa-Aesear > 99%), acetone (Vetec > 99%), ethanol (Vetec > 99%), copper (II) sulphate ($CuSO_4$, Sigma-Aldrich > 99%), indium (III) sulphate ($In_2(SO_4)_3$, Alfa-Aesar 99.99%), gallium (III) sulphate ($Ga_2(SO_4)_3 \cdot 18H_2O$, Alfa-Aesar 99.999%), selenium oxide (SeO_2, Sigma-Aldrich 99.9%), sulphuric acid (H_2SO_4, Alfa-Aesar 98%), sodium nitrate ($NaNO_3$, Vetec 98%) and Triton 100-X (TRT, Vetec > 99%).

Electrochemical experiments were carried out in a potentiostat/galvanostat (Autolab PGSTAT 302 N, Metrohm-Eco Chemie) controlled by GPES® and FRA® softwares. A three-electrode configuration electrochemical cell with a fluorine-doped tin oxide (FTO, 7 ohm/sq, MTI corporation)-coated glass was the working electrode; a Pt-plate served as the auxiliary; and an $Ag/AgCl/Cl^-_{(sat. KCl)}$ served as the reference electrode. The composition and the morphology of the films were evaluated by high-resolution field emission scanning electron microscopy (FE-SEM, Zeiss Supra 35 at 2 kV) and by energy dispersive X-ray (EDX) spectroscopy (FEI XL30 FEG with an Oxford Instruments - Link ISIS 300 detector), respectively. Micro-Raman measurements were made with a Horiba Jobin Yvon (HR 550) system with 514.5-nm wavelength incident argon laser light and coupled with an optical microscope (Olympus BX41) with 10x objective, where the incident laser power was carefully tuned to avoid sample damage or laser-induced heating. The crystallographic film characterisation was performed with the aid of an X-ray diffractometer (Rigaku - DMax 2500PC) with CuKα radiation, a scanning step of 0.02 °, counting time of 6 s, and 2θ range from 20 ° to 120 °. The size of the crystallographic coherence dominium (*D*, nm) was estimated from the (220) CIGSe peak by the Scherrer equation, where the line broadening for the instrumental effects was corrected with silicon powder standard (99%, 325 mesh, SRM-640) based on the Caglioti equation as described by Gonçalves et al. [10]. All samples were refined by the Rietveld method [11] through the GSAS program [12]. The input data of the theoretical model were those available in the Inorganic Crystal Structure Database (ICSD) [13]. NIR-UV-vis spectroscopy with diffuse reflectance geometry was carried out in a Cary 5 E spectrometer from 200 to 2500 nm to determine the band gap energy of the films. The Mott-Schottky experiments were performed in 0.1 mol L^{-1} $NaNO_3$ by applying a 0.01 V_{rms} sinoidal excitation signal with a frequency of 1 kHz.

2.2. Obtaining CIGSe thin films

Initially, by cyclic voltammetry, the electrodeposition process of the elements on FTO was evaluated for use in the study at a concentration of 1 mmol L^{-1}. After the elements were analysed separately, the metals were studied in the presence of Se. Finally, all the elements were studied in the presence of TRT 10 mmol L^{-1}. After studies of the electrochemical deposition potential, the electrodeposition of all films was performed in a stationary bath at −0.80 V versus $Ag/AgCl/Cl^-_{(sat.KCl)}$ for 15 min at 25 °C. For the CIGSe electrochemical deposition, an electrolytic bath contained 4 mmol L^{-1} $CuSO_4$, 2 mmol L^{-1} $In_2(SO_4)_3$, 10 mmol L^{-1} $Ga_2(SO_4)_3$, 8 mmol L^{-1} SeO_2, and 0.3 mol L^{-1} Na_2SO_4/H_2SO_4 with pH 1.5 (as supporting electrolyte) and different additive concentrations (0.1, 1.0, and 10 mmol L^{-1}). FTO was cleaned ultrasonically with isopropanol, acetone and ethanol for 15 min, in each solvent, then rinsed with deionised water and dried in an $N_{2(g)}$ stream prior to deposition. To improve crystallinity of the electrodeposited CIGSe, the films were annealed at 450 °C for 1 h into a sealed lead borosilicate glass cylinder (volume 300 mL). For this thermic treatment, a tube furnace was used with a constant flow of nitrogen (10 cm^3 min^{-1}).

3. Results and discussion

3.1. Electrochemical deposition potential

First, the electrochemical behaviour of the individual Cu^{2+}, In^{3+}, Ga^{3+} and $HSeO_3^-$ ions in the 0.5 mol L^{-1} H_2SO_4 solution (the supporting electrolyte, SE) on the FTO surface were analysed using cyclic voltammetry and the cyclic voltammograms (CV) can be seen in Fig. 1.

Fig. 1 is a cyclic voltammogram of a clean FTO substrate in H_2SO_4 0.5 mol L^{-1} (Supporting Electrolyte, SE) + 1 mM Cu^{2+}. In the presence of copper ions two cathodic and two anodic peaks are observed. The cathodic peak C_1 could be related to the reduction of Cu^{2+} to Cu^+ and C_2 to reduction of Cu^+ to Cu^0 [14]. At more negative potential, the cathodic current increases exponentially due to hydrogen formation. The first anodic peak A_2 is associated with the

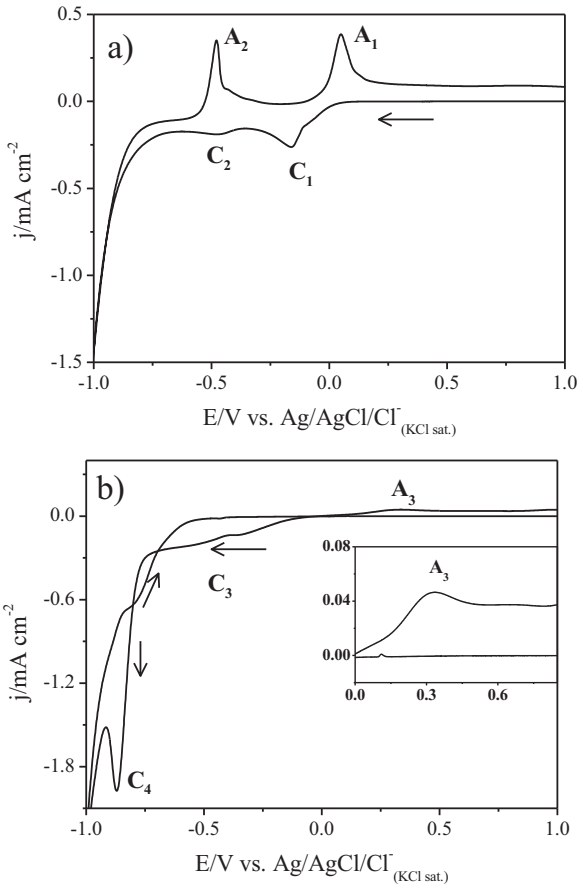

Fig. 1. Cyclic voltammograms on FTO and at a scan rate of 50 mV s^{-1} for H_2SO_4 0.5 mol L^{-1} + 1 mmol L^{-1} solutions of a) Cu^{2+} and b) $HSeO_3^-$ (in insert, expansion of the region from 0 to 0.9 V).

oxidation of Cu^0 to Cu^+ and peak A_1 to the oxidation of Cu^0 to Cu^{2+}. Similar behaviour was observed by Liu et al. [14]. In the cyclic voltammograms of Fig. 1b, the electrochemical behaviour of the selenium species on the FTO substrate allow identification of two cathodic peaks (C_3 e C_4) in the direct scan and one anodic peak (A_3) in the inverse scan. These electrochemical processes are consistent with previous reports noting that the kinetics of selenite in aqueous solutions is slow and complex [15]. The broad peak starting at −0.1 to −0.7 V, C_3, can be categorised as overpotential deposits; anodic peak A_3 is attributed to the dissolution of these deposits. When more potential is swept, the reduction peak C_4 results from a Se reduction to H_2Se (a soluble species), as well as some extensive hydrogen evolution. The reaction observed for Se ions can be summarised according to the following reactions, where the processes C_3 and A_3 can be associated with Eq. 1 and the C_4 with Eq. 2 and Eq. 3. [14,16]:

$$H_2SeO_{3(aq)} + 4H^+_{(aq)} + 4e^- \leftrightarrows Se_{(s)} + 3H_2O_{(l)} \quad (1) \qquad (1)$$

$$H_2SeO_{3(aq)} + 6H^+_{(aq)} + 6e^- \leftrightarrows H_2Se_{(aq/g)} + 3H_2O_{(l)} \quad (2) \qquad (1)$$

$$Se_{(s)} + 2H^+_{(aq)} + 2e^- \leftrightarrows H_2Se_{(aq/g)} \quad (3) \qquad (3)$$

Under this study's experimental conditions, neither cyclic voltammetry peaks of reduction nor oxidation of the In^{3+} and Ga^{3+} were observed in the potential range. However, in the cyclic voltammograms obtained in presence of these ions, a shift in the anodic peak was observed and attributed to a substrate of more negative potential value. This behaviour could be considered indicative of these ions being incorporated into the crystalline matrix of the substrate.

After the study of the separated ions, the voltammetric behaviour of each ion (Cu^{2+}, In^{3+} and Ga^{3+}) was observed in the presence of $HSeO_3^-$. The electrochemical behaviour of these binary systems can be seen in Fig. 2.

Fig. 2a represents CVs obtained in the mixture of Cu^{2+} and $HSeO_3^-$ ions, demonstrating two cathodic peaks and three anodic peaks. The first cathodic peak is denominate C_1 because it occurs at the same potential as in Fig. 1a. The second enlarged cathodic peak at−0.38 V, called C_5, can be attributed to the combination of the C_2 and C_3 processes and the following reactions [14,16]:

$$2Cu^{2+}_{(aq)} + H_2SeO_{3(aq)} + 4H^+_{(aq)} + 6e^- \leftrightarrows Cu_2Se_{(s)} + 3H_2O_{(l)} \quad (4) \qquad (1)$$

$$Cu^{2+}_{(aq)} + H_2SeO_{3(aq)} + 4H^+_{(aq)} + 6e^- \leftrightarrows CuSe_{(s)} + 3H_2O_{(l)} \quad (5) \qquad (1)$$

$$Cu_2Se_{(s)} + CuSe_{(s)} \leftrightarrows Cu_3Se_{2(s)} \quad (6) \qquad (6)$$

During anodic sweep, the peak at 0.0 V occurs at the same potential of peak A_1 (Fig. 1a), but its current is a very low mixture, indicating that the presence of a pure Cu phase is not preferentially deposited in this case. The more pronounced anodic peak appears at 0.25 V (peak A_5) and cannot be associated with any process observed for Cu or Se pure, so this peak was attributed to the Cu_xSe_y phase dissolution. Fig. 2a also demonstrates that the reduction of Se to H_2Se no longer occurs when there is a codeposition of metals, indicating that Se is more stable when the compound Cu_xSe_y is formed. In the mixture of ions, the hydrogen evolution reaction shifts at less negative potential, and the peak A_4 observed during the anodic sweep could be due to the oxidation of hydrogen [14]. The same behaviour is observed when Se is deposited in the presence of In^{3+} (Fig. 2b). In this case the process C_4, previously observed in Fig. 1b, is no longer seen. In the inverse scan, an anodic process (A_6) was observed and can be

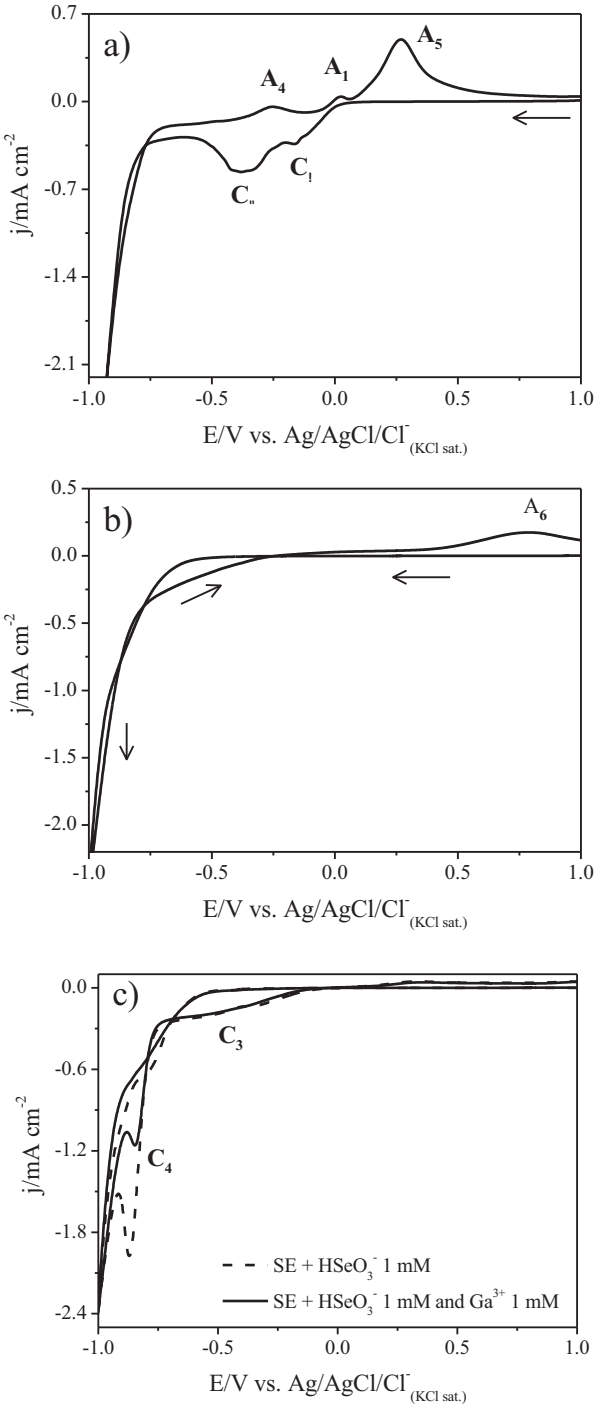

Fig. 2. Cyclic voltammograms on FTO and at scan rate of 50 mV s^{-1} for solutions of $HSeO_3^-$ 1 mmol L^{-1} with 1 mmol L^{-1} of a) Cu^{2+}, b) In^{3+} and c) Ga^{3+} (in dashed lines, only $HSeO_3^-$ 1 mmol L^{-1}) in H_2SO_4 0.5 mol L^{-1} (as supporting electrolyte, SE).

attributed to the In_2Se_3 phase oxidation, likely due to the following reaction [14,16]:

$$3H_2Se_{(aq/g)} + 2In^{3+}_{(aq)} \leftrightarrows In_2Se_{3(s)} + 6H^+_{(aq)} \quad (7) \qquad (7)$$

$$3Se_{(s)} + 2In^{3+}_{(aq)} + 6e^- \leftrightarrows In_2Se_{3(s)} \quad (8) \qquad (8)$$

In the other side, for mixture of $HSeO_3^-$ and Ga^{3+}, the peak C_4 maintains, but its intensity is reduced by nearly half (see Fig. 2c) and no anodic peak appears in this case. These facts imply that if

the deposition of a GaSe phase occurs, it occurs at a very low proportion. According some authors, during Ga and Se codeposition the Ga_2Se_3 phases can be formed, following these reactions [14,16]:

$$3H_2Se_{(aq/g)} + 2\,Ga^{3+}{}_{(aq)} \leftrightarrows Ga_2Se_{3(s)} + 6H^+{}_{(aq)} \quad (9)$$

$$3Se_{(s)} + Ga^{3+}{}_{(aq)} + 6e^- \leftrightarrows Ga_2Se_{3(s)} \quad (10)$$

Finally, all ions were studied together in the presence of Triton 100-X (TRT) 10 mmol L^{-1}. The electrochemical behaviour of this quaternary system, in the absence and presence of the studied additive, can be seen in Fig. 3.

Due to the complexity of this system, in which are possible the different redox processes of pure metals and the formation of binary, ternary or quaternary compounds, we chose not to do assignments to cathodic and anodic peaks observed in Fig. 3 at one specified process. However, four cathodic processes in the direct scan and two anodic processes in the inverse scan are clear in all voltammograms. There was no significant peak potential shift in these processes in the presence of the additive, proving that the additives do not form complexes with ions of the electrolytic bath. One interesting fact to be highlighted is the increase in the intensity of the peak at 0.52 V in the presence of the additive. The difference in peak potential of individual and binary processes could relate to the formation of a ternary or quaternary phase, and one can conclude that deposition of this phase favours the presence of additive. After studying the electrochemical behaviour, the potential of -0.8 V was chosen for the electrodeposition of the CIGSe films, which favours the formation of the In, Ga and Cu selenides according to the chemical and electrochemical reactions shown above. The films obtained were characterized using different techniques.

3.2. Surface properties and film composition

The morphological characteristics of the CIGSe electrodeposited films were observed by scanning electron microscopy (SEM). The SEM micrographs of the film obtained from the bath without an additive are shown in Fig. 4 at different magnifications. Fig. 4a shows two different morphologies. One inferior layer is more homogenous and formed by globular structures; a superior layer constituted of clusters. Magnifying the clusters region demonstrates that it is formed by lamellar structures. Similar morphologies were observed in presence of different concentrations of Triton 100-X.

Fig. 5 shows SEM micrographies at a higher magnification of globular structures in the absence and presence of 0.1, 1.0 and 10 mM of TRT. The effect of the additive concentration on the morphological characteristics of the CIGSe films was also interesting. Fig. 5 demonstrates that the additive promotes changes in the film's grain size, despite all films having a globular aspect. The film obtained at 10 TRT had an apparently more compact morphology and small grains.

Associated with SEM, semiquantitative analyses of the film composition were carried out by energy-dispersive X-ray spectroscopy (EDX), and the data are organised in Table 1.

Table 1 demonstrates that the composition of deposits changes only slightly when 0.1 mM TRT is added to the deposition bath. For samples obtained from solutions with 1.0 and 10 TRT, the film composition is similar; the percentage of Cu increases and that of Se and In decreases. The films' stoichiometry is approximately $CuInSe_2$ and $CuIn_2Se_2$ for deposits with 1.0 and 10 TRT and without additive and 0.1 TRT, respectively. The Ga percentage is very small for all samples, what could be indicative that deposits contain ternary $CISe_2$ films doped with Ga. This result is consistent with the voltammograms in Fig. 2c, as Ga was deposited in a low proportion.

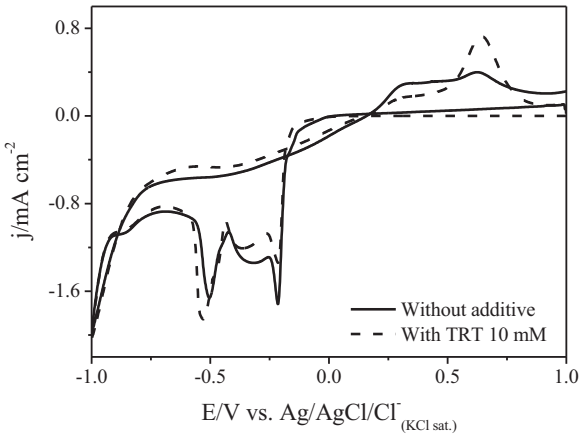

Fig. 3. Cyclic voltammograms on FTO and at scan rate of 50 mV s^{-1} for the solution consisting of $HSeO_3^-$, Cu^{2+}, In^{3+} and Ga^{3+} (1 mmol L^{-1}, each) in H_2SO_4 0.5 mol L^{-1}. In the absence of the additive (solid line) and containing TRT 10 mmol L^{-1} (dashed line).

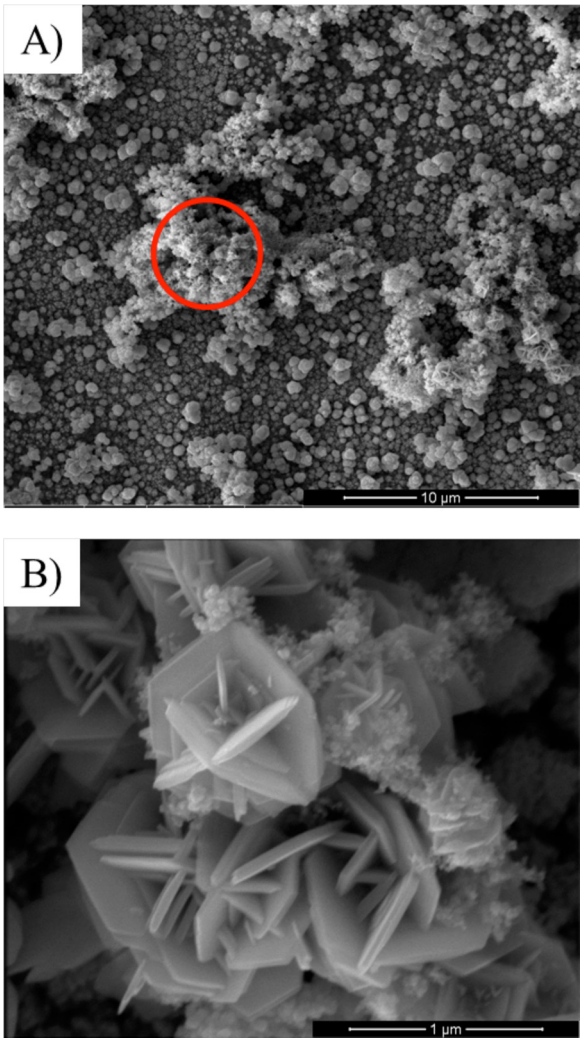

Fig. 4. SEM micrographs of NADT-CIGSe film with magnification of a) 10,000 X and b) 100,000X of the red circled region in Figure a.

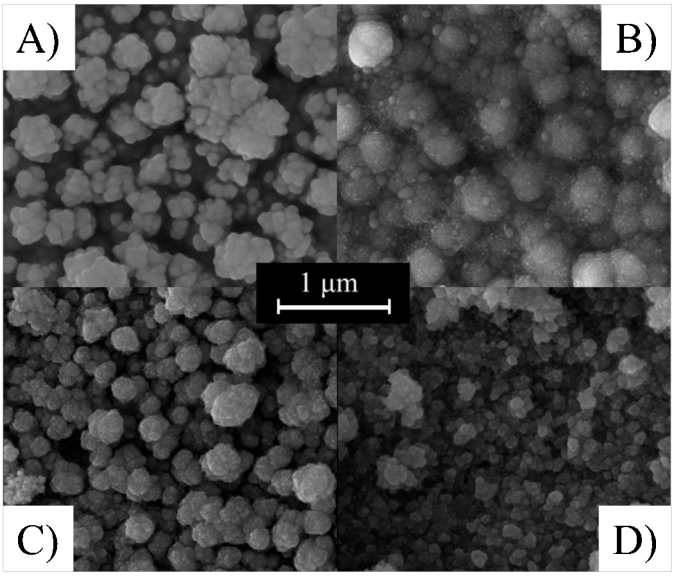

Fig. 5. SEM micrographs with magnification of 100,000X of the CIGSe films a) NADT, b) 0.1TRT, c) 1TRT and d) 10TRT.

To characterise the physical properties of these films, the flat band potential (E_{fb}), the charge carriers density (N_D) and the semiconductor type (n- or p-) were determined by Mott-Schottky equation. The flat band potential allows locating the energetic position of the valence and conduction band edge of a given semiconductor material. The results obtained by potentiodynamic electrochemical impedance spectroscopy experiment are described by the following equation [17–19]:

$$\frac{1}{C_{SC}^2} = \frac{2}{eN_D\varepsilon_0\varepsilon_s}\left[(E - E_{fb}) - \frac{k_BT}{e}\right] \quad (11)$$

where C_{SC} is the semiconductor capacitance of the space charge region, ***e*** the elementary charge, N_D the charge carriers density, ε_0 the permittivity of free space, ε_s the semiconductor dielectric constant, E the applied potential, E_{fb} the flat band potential, k_B the Boltzmann constant and T the absolute temperature.

Using a Mott-Schottky graph, the N_D can be calculated from the slope and the E_{fb} can be obtained from the extrapolation to $C_{SC}^{-2} = 0$. The thin films were prepared, and capacitance data were obtained in 0.1 mol L^{-1} $NaNO_3$ by applying a 0.01 V_{rms} sinoidal excitation signal with a frequency of 1 kHz. The Mott-Schottky graph for the 1TRT film and N_D and E_{fb} values can be seen in Fig. 6. The same behaviour was observed in other experimental condition studied in the absence of an additive and in the presence of 0.1 mM and 10 mM of TRT. The data obtained from Mott-Schottky are given at Table 1.

Table 1
Perceptual atomic composition, flat-band potential (Efb), charge carriers density (ND) of the CIGSe films.

CIGSe	Atomic composition (% atm.)				Mott-Schottky	
	Cu	In	Ga	Se	E_{fb} (V)*	N_D (cm^{-3})**
NADT	10	23	1.2	66	-0.92	5.37×10^{20}
0.1TRT	9	27	1.8	62	-0.90	4.57×10^{21}
1TRT	17	18	3.3	62	-0.67	4.45×10^{19}
10TRT	19	17	2.7	62	-1.27	1.27×10^{22}

* E vs. $Ag/AgCl/Cl^-_{(KClsat.)}$.
** For calculation was used $\varepsilon_S = 13.5$ [29].

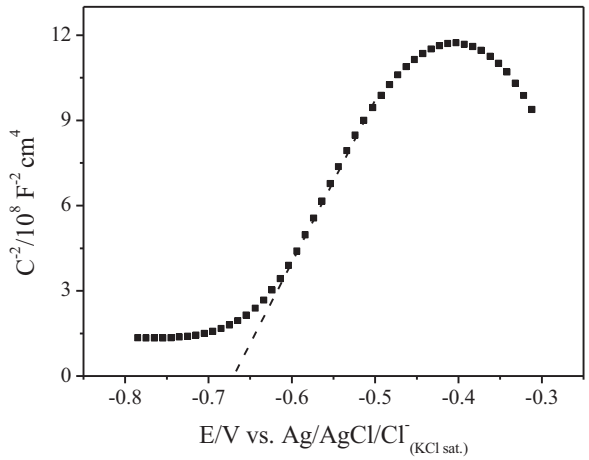

Fig. 6. Mott-Schottky graph, using frequency of 1 kHz and performed in $NaNO_3$ 0.1 mol L^{-1} by applying a sinusoidal excitation of 0.01 V_{rms} for the 1TRT film.

Based on the slope of the Mott-Schottky graph, all obtained films were n-type semiconductors because the slope was positive in all cases [17–19]. This behaviour is expected for doped CIGSe films, as observed by Djellal et al. [20]. In this work, E_{fb} measured was in range of–0.90 to–1.27 V versus $Ag/AgCl/Cl^-_{(sat.KCl)}$, and this value shifted more negative potential when 10 TRT was added in the bath deposition.

Comparing the N_D values in the absence and presence of additives, it is possible to see that N_D increases at deposit growth of 0.1 and 10 TRT but decreases when the additive concentration is 1.0 TRT. The 1TRT film showed N_D and E_{fb} values closer to those reported in the literature on CIGSe films that is, this film had an electronic structure closer to that obtained by this good quality method. The high N_D observed for 10 TRT electrodeposits could be due to small clusters observed by SEM on the film's surface. These structures could be constituted by secondary phases as Cu_xSe_y, which could increase the defect's density on the surface, causing the high N_D values observed, as argued by Valdés et al. [21]. Because the Mott-Schottky plot primarily describes the electronic behaviour on the surface [22], we can conclude that the 1TRT film had fewer surface defects than the NADT film. Assumptions about the possible secondary phases in deposits to explain the ND values can be proven by the XRD analysis presented below.

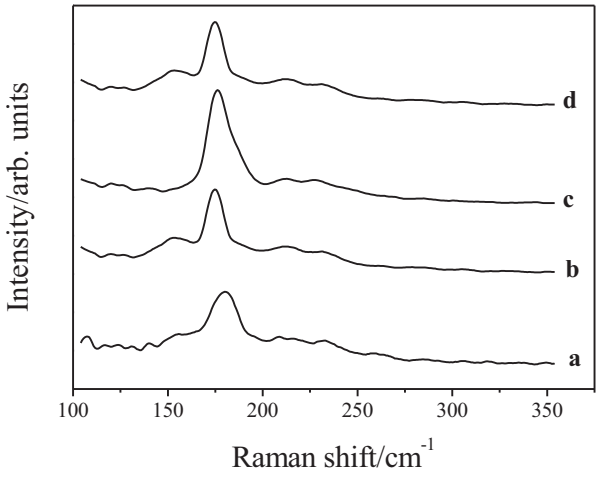

Fig. 7. Raman spectrum of the CIGSe films a) NADT, b) 0.1TRT, c) 1TRT and d) 10 TRT.

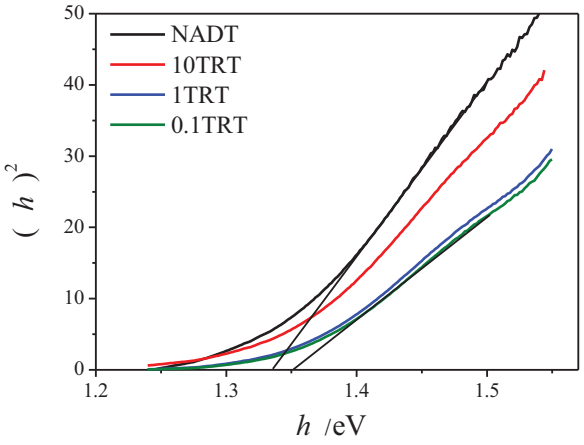

Fig. 8. Experimental and calculated X-ray diffraction patterns of the NADT and 1TRT films.

3.3. Structural properties (bulk properties)

To prove and identify the phase formation, the CIGSe films were characterised by Raman spectroscopy and by X-ray Diffraction (XRD). The Raman spectra and the diffraction patterns of the CIGSe films can be seen in Figs. 7 and 8, respectively.

For all films, a well-defined peak at about 174 cm^{-1} was observed which can be attributed to the A_1 symmetry vibrational mode of CIGSe resulting from the Se atom motion in the *x-y* plane with other atoms at rest [23–27]. The smallest full width at half maximum (FWHM) of the 174 cm^{-1} peak was observed for the films 0.1 and 1TRT, evidencing that these had a greater level of bulk crystallinity (the data can be seen in Table 2). Shoulders in the region of 213 to 230 cm^{-1} were observed, which could be related to the mixing of phonon modes of B_2 and E symmetries of the chalcopyrite phase [23]. In the Raman spectrum of the films NADT 0.1 TRT and 1TRT, a shoulder was also observed at about 154 cm^{-1}, possibly due to the formation of ordered vacancies compounds (OVCs) attributed to the existence of complex point defects in the chalcopyrite structure [25]. There was no evidence of the presence of bands associated with elemental Se, around 240 cm^{-1}, or to Cu_xSe_y phases in the region of 258 cm^{-1} [23–27], but this does not mean that these phases are not present. The high Raman scattering of the majority phase (CIGSe) could have suppressed the secondary phases.

In addition to the conclusions obtained from the Raman spectrum and to verify the presence of secondary phases, Rietveld refinement (RR) of the CIGSe film diffraction patterns was performed. Fig. 8 shows the experimental and calculated X-ray diffraction patterns from refinements made by the Rietveld method of the NADT and 1TRT films. Most of the qualitative and statistical results obtained by RR are summarised in Table 2.

In all refinements, the R_{BRAGG} index presented satisfactory low values, indicating a good refined crystal structure model representative of the real case. The residual pattern shows that there is a good match between the theoretical and observed XRD patterns, noted by the small variation along the diffraction angle as shown in Fig. 6, as is also evidenced by the R_{wp} and χ^2 index values shown in Table 2. Thus, by comparison with patterns available in the Inorganic Crystal Structure Database (ICSD) [13], it was observed that the majority phase present in all films was the CIGSe [ICSD code: 163564, space group: I -4 2 m (121)]. Secondary phases not identified in the Raman spectra were also observed, such as Cu_2Se [ICSD code: 59955, space group: F 2 3(196)], In_2Se_3 [ICSD code 1376, space group P 61(169)] and Se [ICSD code: 24635, space group: P 1 21/c 1(14)]. Table 2 demonstrates the phases present in each film. Only the 1TRT film did not present bulk secondary phases. From (2 2 0) the peak of the majority phase, the size of the crystallographic coherence dominium (*D*) of the films was estimated, and the data are organised in Table 2. As observed based on the Raman spectra, one of the less crystalline films was NADT that is, it has a smaller D. The more crystalline films were the 0.1 and 1TRT; the use of the additive improved the crystallinity of the films, one of the more important properties required for films to be applicable in photovoltaic devices. The band-gap energy (E_g) of the films was determined by NIR-UV-Vis diffuse reflectance spectroscopy (DRS) using the following equation [28]:

$$\alpha = F(R) = \frac{(1-R)^2}{2R} \text{and} (\alpha h\nu)^n = A(h\nu - E_g) \quad (12)$$

where *F(R)* is the Kubelka-Munk function, *R* is the absolute reflectance to a given value of $h\nu$, α is the absorption coefficient, *h* Planck constant, ν is the frequency, and *n* assumes the values of 2 or 2/3 for direct transition (allowed and forbidden, respectively) and 1/2 or 1/3 for indirect (allowed and forbidden, respectively).

Fig. 9 shows the graphs of $(\alpha h\nu)^2$ as a function of $h\nu$; the E_g values were determined by extrapolating the linear region, as shown in Equation 12, for an allowed direct transition (i.e., *n* equals 2). The E_g of the films are organised in Table 2.

The values of E_g found at about 1.35 eV (see Table 2) are compatible with CIGSe E_g as described in the literature [15]. For the $CuInSe_2$ system, the value of E_g would be about 1.04 eV [4], a value much lower than that obtained in our work. This shows that despite the EDX, results indicate the formation of a film-type doped Ga-CISe2, and optical and structural parameters demonstrated that the Ga content was sufficient for the formation of CIGSe phases.

Summarising all previous characterisations, the NADT and 10TRT films present a greater number of secondary phases and

Table 2
Phases identified, Rietveld refinement (RR) parameters, size of crystallographic coherence dominium (*D*), full width at half maximum (FWHM) and band gap energy for the CIGSe films.

CIGSe	Phases*				RR parameters			D (nm)	FWHM (cm^{-1})	E_g (eV)
	CIGSe (majority)	CuSe	InSe	Se	R_{wp} (%)	R_{bragg} (%)	χ^2			
NADT	X	X	–	X	3.08	1.03	3.05	14.98	14.7	1.34
0.1TRT	X	X	X	–	7.17	9.80	4.47	26.05	9.55	1.33
1TRT	X	–	–	–	6.54	7.47	3.75	22.13	10.2	1.35
10TRT	X	X	X	–	13.0	8.46	10.3	16.28	14.9	1.34

* ICSD code phases: CIGSe (163564), CuSe (59955), InSe (1376) and Se (24635). The FTO (SnO_2 cassiterite phase, 90611) phase was present in all films. D was calculated from the (220) peak and FWHM from A_1 mode of the CIGSe phase.

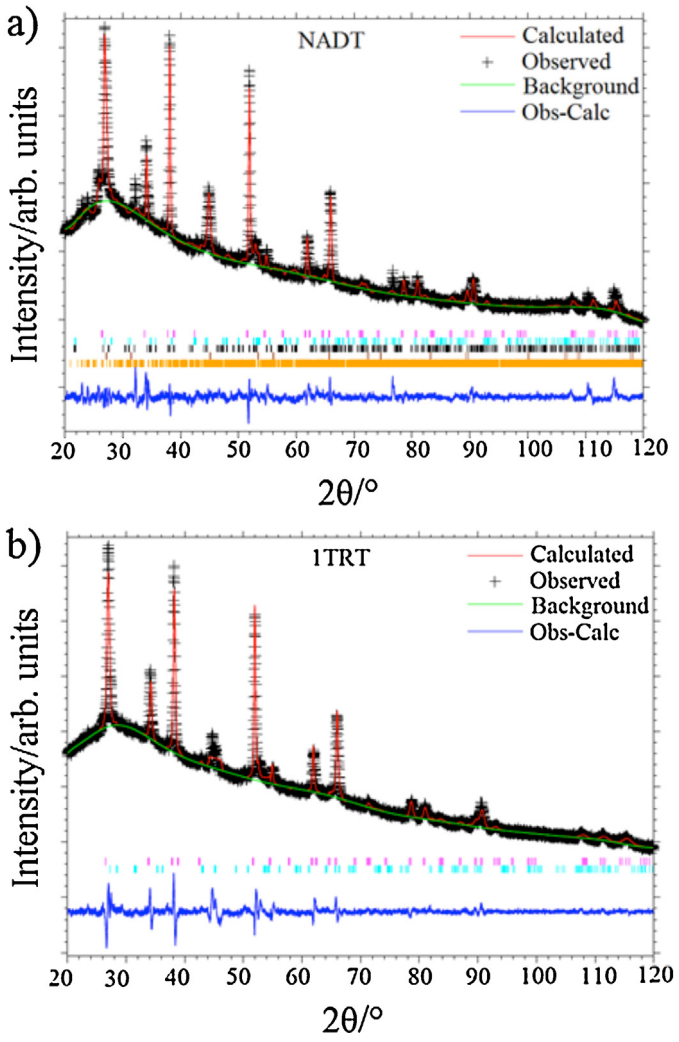

Fig. 9. Graph of $(\alpha h\nu)^2$ versus $h\nu$ for the CIGSe films.

lower bulk crystallinity, which justifies the high surface defect level (identified by the value of N_D) and explains why E_{fb} is so different from the other films (see Table 2). In contrast, the optimised condition of electrodeposition was achieved with the use of 1 mM TRT in electrolytic bath, explaining the reduction of the number of surface defects, secondary phases and the increase of the size of crystallographic coherence dominium and the crystallinity of the CIGSe film.

4. Conclusions

The simple addition of nonionic and noncomplexing additive can change a film's morphology/microstructure, creating interesting effects in their electronics properties. All characterisations led to the conclusion that compared to CIGSe, film obtained without an additive and in the presence of 1 mM Triton 100-X reduces the number of surface defects and improves the bulk crystallinity of the electrodeposited CIGSe films. It was also observed that the addition of 1 mM Triton 100-X in the deposition baths inhibits the formation of secondary phases in the electrodeposited films.

Acknowledgments

The authors wish to thank the São Paulo Research Foundation (FAPESP), grant 2012/10947-2, 2013/07296-2 and INCTMN 2008/57872-1CNPq 573636/2008-7.

References

[1] G. Hodes, Physical electrochemistry: principles, methods and applications, Marcel Dekker Inc., New York, 1995.
[2] V.S. Saji, I.-H. Choi, C.-W. Lee, Progress in electrodeposited absorber layer for $CuIn_{(1-x)}Ga_xSe_2$ (CIGS) solar cells, Sol. Energy. 85 (2011) 2666.
[3] L. Djellal, S. Omeiri, A. Bouguelia, M. Trari, Photoelectrochemical hydrogen-evolution over p-type chalcopyrite $CuInSe_2$, J. Alloys Compd. 476 (2009) 584.
[4] D. Lincot, J.F. Guillemoles, S. Taunier, D. Guimard, J. Sicx-Kurdi, A. Chaumont, et al., Chalcopyrite thin film solar cells by electrodeposition, Sol. Energy. 77 (2004) 725.
[5] R.N. Bhattacharya, Electrodeposited two-layer Cu–In–Ga–Se/In–Se thin films, J. Electrochem. Soc. 157 (2010) D406.
[6] R.N. Bhattacharya, 12.3% efficient $CuIn_{1-x}Ga_xSe_2$-based device from electrodeposited precursor, J. Electrochem. Soc. 144 (1997) 1376.
[7] R.N. Bhattacharya, 14.1% $CuIn_{1-x}Ga_xSe_2$-based photovoltaic cells from electrodeposited precursors, J. Electrochem. Soc. 145 (1998) 3435.
[8] R.N. Bhattacharya, W. Batchelor, J.F. Hiltner, J.R. Sites, Thin-film $CuIn_{1-x}Ga_xSe_2$ photovoltaic cells from solution-based precursor layers, Appl. Phys. Lett. 75 (1999) 1431.
[9] Y.A. Qin, A. Wassay, C. Liu, G.D. Wilcox, K. Zhao, C. Wang, Electrodeposition of Sn-Cu solder alloy for electronics interconnection, International Conference on Electronic Packaging Technology and High Density Packaging (2009) 772.
[10] N.S. Gonçalves, J.A. Carvalho, Z.M. Lima, J.M. Sasaki, Size–strain study of NiO nanoparticles by X-ray powder diffraction line broadening, Mater. Lett. 72 (2012) 36.
[11] R.A. Young, The Rietveld method, Oxford University Press, London, 1995.
[12] R.B.V.-D.A.C. Larson, General Structure Analysis System (GSAS) (1994) .
[13] Inorganic Crystal Structure Database, last accessed date 27th July 2014, available at: http://www.fiz-karlsruhe.de/icsd.html.
[14] J. Liu, F. Liu, Y. Lai, Z. Zhang, J. Li, Y. Liu, Effects of sodium sulfamate on electrodeposition of Cu(In,Ga)Se_2 thin film, J. Electroanal. Chem. 651 (2011) 191.
[15] D. Banga, N. Jarayaju, L. Sheridan, Y. Kim, B. Perdue, X. Zhang, et al., Electrodeposition of $CuInSe_2$ (CIS) via electrochemical atomic layer deposition (E-ALD), Langmuir 28 (2012) 3024.
[16] M. Dergacheva, K. Urazov, Electrodeposition of $CuIn_xGa_{1-x}Se_2$ thin films from sulfosalicylic acid, Electrochim. Acta 107 (2013) 120.
[17] K. Gelderman, L. Lee, S.W. Donne, Flat-band Potential of a semiconductor: using the Mott– Schottkyequation, J. Chem. Educ. 84 (2007) 685.
[18] W.J. Albery, G.J. O'shea, A.L. Smith, Interpretation and use of Mott-Schottky plots at the semiconductor/electrolyte interface, J. Chem. Soc. Faraday Trans. 92 (1996) 4083.
[19] A.W. Bott, Electrochemistry of semiconductors, Curr. Sep. 17 (1998) 87–91.
[20] L. Djellal, M. Doulache, M. Trari, Photoelectrochemical properties of Cu$(In_{0.75}Ga_{0.25})_3Se_5$ ordered vacancy compound, Semicond. Sci. Technol. 26 (2011) 85034.
[21] M.H. Valdés, M. Vázquez, Pulsed electrodeposition of p-type $CuInSe_2$ thin films, Electrochim. Acta 56 (2011) 6866.
[22] P. Sebastian, M. Calixto, R. Bhattacharya, R. Noufi, CIS and CIGS based photovoltaic structures developed from electrodeposited precursors, Sol. Energy Mater. Sol. Cells 59 (1999) 125.
[23] A. Bhatia, H. Meadows, W.M. Hlaing Oo, P.J. Dale, M.A. Scarpulla, Effects of pulsed laser annealing on deep level defects in electrochemically-deposited and furnace annealed $CuInSe_2$ thin films, Thin Solid Films 531 (2013) 566.
[24] O. Ramdani, J.F. Guillemoles, D. Lincot, P.P. Grand, E. Chassaing, O. Kerrec, et al., One-step electrodeposited $CuInSe_2$ thin films studied by Raman spectroscopy, Thin Solid Films 515 (2007) 5909.
[25] Y.-H. Su, T.-W. Chang, W.-H. Lee, B.-H. Tseng, Characterization of $CuInSe_2$ thin films grown by photo-assisted electrodeposition, Thin Solid Films 535 (2013) 343.
[26] M. Valdés, M. Mollar, M. Vázquez, B. Marí, Pulsed and potentiostatic electrodeposition of $CuInSe_2$ on gold-coated alumina substrates, J. Appl. Electrochem. 43 (2013) 619.
[27] M. Valdés, M. Vázquez, Composition, morphology, and optical properties of $CuInSe_2$ thin films electrodeposited using constant and pulsed potentials, J. Solid State Electrochem. 16 (2012) 3825.
[28] M. Nowak, B. Kauch, P. Szperlich, Determination of energy band gap of nanocrystalline SbSI using diffuse reflectance spectroscopy, Rev, Sci. Instrum. 80 (2009) 046107.
[29] T. Minemoto, H. Matsui, Y. Takakura, T. Hamakawa, Y. Negami, T. Hashimoto, M. Uenoyama, Theoretical analysis of the effect of conduction band offset of window/CIS layers on performance of CIS solar cells using device simulation, Sol. Energy Mater. Sol. Cells 67 (2001) 83.